IEEE Access
Multidisciplinary | Rapid Review | Open Access Journal

SPECIAL SECTION ON INTELLIGENT AND COGNITIVE TECHNIQUES FOR INTERNET OF THINGS

Received September 4, 2019, accepted October 5, 2019, date of publication October 14, 2019, date of current version October 28, 2019.

Digital Object Identifier 10.1109/ACCESS.2019.2947169

Fast and Refined Processing of Radar Maneuvering Target Based on Hierarchical Detection via Sparse Fractional Representation

XIAOLONG CHEN, (Member, IEEE), JIAN GUAN, (Member, IEEE), GUOQING WANG, HAO DING, AND YONG HUANG

Radar Target Detection Research Group, Naval Aviation University, Yantai 264001, China

Corresponding author: Xiaolong Chen (cxlcxl1209@163.com)

This work was supported in part by the National Natural Science Foundation of China under Grant U1933135, Grant 61871391, Grant 61931021, Grant U1633122, and Grant 61871392, in part by the National Defense Science Foundation under Grant 2102024, in part by the Key Research and Development Program of Shandong under Grant 2019GSF111004, and in part by the Special Funds of Young Talents Program of CAST under Grant YESS20160115.

ABSTRACT Reliable and fast detection of maneuvering target in complex background is important for both civilian and military applications. It is rather difficult due to the complex motion resulting in energy spread in time and frequency domain. Also, high detection performance and computational efficiency are difficult to balance in case of more pulses. In this paper, we propose a fast and refined processing method of radar maneuvering target based on hierarchical detection, utilizing the advantages of moving target detection (MTD), and the proposed sparse fractional representation. The method adopts two-stage threshold processing. The first stage is the coarse detection processing screening out the rangebins with possible moving targets. The second stage is called the refined processing, which uses robust sparse fractional Fourier transform (RSFRFT) or robust sparse fractional ambiguity function (RSFRAF) dealing with high-order motions, i.e., accelerated or jerk motion. And the second stage is carried out only within the rangebins after the first stage. Therefore, the amount of calculation can be greatly reduced while ensuring high detection performance. Finally, real radar experiment of UAV target detection is carried out for verification of the proposed method, which shows better performance than the traditional MTD method, and the FRFT-FRAF hierarchical coherent integration detection with less computational burden.

INDEX TERMS Radar maneuvering target detection, hierarchical detection, sparse fractional Fourier transform (SFRFT), sparse fractional ambiguity function (SFRAF), sparse fractional representation.

I. INTRODUCTION

As the main means of target detection and surveillance, radar is widely used in civilian and national defense security fields, such as air and marine target monitoring and early warning detection [1]. Affected by the clutter environment and the complex motion characteristics of targets, the radar returns of moving target are extremely weak and complex resulting in low observability, which makes it difficult for radar to detect, especially for the maneuvering target [2]. Reliable, fast detection and estimation techniques for maneuvering targets in complex backgrounds have become the key constraints of radar performance. With the development of signal processing, radar has the ability to acquire refined target features [3]. By extending the signal dimensions, it provides a new way to further improve the detection and recognition of radar maneuvering targets. However, there are still several difficulties for radar maneuvering target detection at present, which can be summarized as follows.

1) The signal-to-clutter ratio (SCR) of the maneuvering target is usually low with non-stationary characteristics. The echoes have high-order phase and time-varying frequency characteristics, and the traditional filter-based method, i.e., moving target detection (MTD) is more suitable for analyzing uniform moving targets. For maneuvering target detection [4], the accumulated echo spectrum will span multiple Doppler units, i.e., Doppler frequency migration (DFM). Therefore, the energy is divergent, which is difficult to achieve coherent integration in one Doppler

The associate editor coordinating the review of this manuscript and approving it for publication was Min Jia.

bin. The detection performance would degrade accordingly [5]–[8].

2) Radar moving target detection methods based on time-frequency distribution (TFD) extend one-dimensional frequency domain processing to two-dimensional time-frequency processing, which can reflect the Doppler changes with time [9]. These methods can be regarded as the extension of traditional MTD method, such as short-time Fourier transform (STFT), Wigner-Vill distribution (WVD), etc., which have been used in feature extraction, target imaging, and recognition [10]. However, there are still some problems, such as low time-frequency aggregation level, limited resolution, and partially affected by cross-terms, which makes it difficult to meet the actual radar requirements. In addition, most of the methods are signal matching enhancement methods, which means they need to match the target motion characteristics, but in reality, the moving target signal is complex and the accumulated gain would decrease accordingly.
3) By using a phased array radar or multiple-input and multiple-output (MIMO) radar [11], the observation time can be prolonged to obtain more pulses on target increasing the target's energy accordingly. Therefore, the refined description ability of the moving target can be improved [12]. However, the long integration time and the high sampling frequency greatly increase the number of echo pulses [13]. The algorithm would cost a huge computational burden, consuming a large amount of radar signal processing resources. That is to say high detection performance and computational efficiency are difficult to balance.

Therefore, it is urgent to develop and study fast and reliable detection methods suitable for maneuvering targets, and to accurately estimate the motion status and parameters. Thereby it would lay a foundation for the refined description of the maneuvering target for further processing.

The traditional MTD method can be realized based on fast Fourier transform (FFT), which has certain advantages in computational efficiency, but it is not suitable for maneuvering target with time-varying characteristics. The Doppler spectrum would be widened and the detection performance is degraded. The fractional transform methods employ chirp signal as the composition basis, and the fractional domain representation between the time domain and the frequency domain can reflect the variation of Doppler. It is very suitable for time-varying signals without cross-terms interference. The popular transform is fractional FT (FRFT) [14], [15] and fractional ambiguity function (FRAF) [2], etc.. However, it is difficult to adapt to large-scale radar echo processing due to the two-dimensional parameter searching, which is time consuming. Moreover, the time-frequency resolution is limited by the searching intervals and the transform itself.

In recent years, a series of sparse signal processing technologies have emerged and developed [16]–[19]. Among them, the sparse FT (SFT) method proposed by scholars of the Massachusetts Institute of Technology (MIT) was selected as the top ten disruptive technologies in 2012 by MIT Technical Review [20], [21]. The core idea of the SFT algorithm is to convert the N-point long sequence into the B-point short sequence and then perform the FT, which is more efficient than the traditional FFT. For a sparse N-point size input signal, the computational complexity of SFT can be reduced to $O(K \log N)$ compared with FFT, where K is called as the sparsity, i.e., the number of large-valued coefficients in the frequency domain [22], [23]. Ref [24] proposed a method for high-speed target detection based on SFT. However, the SFT needs to know signal sparsity in advance, which is impossible and unrealistic. Therefore, lots of work study the robust SFT or its enhancement solution for real applications [25], [26]. However, most of the methods are mainly for signal processing in noise background, and the SFT is easily affected by strong clutter. Ref [27] designed an adaptive dual-threshold SFT (ADT-SFT) algorithm, which is used for uniformly moving target detection in clutter environment.

On the basis of the SFT theoretical framework, [28] redesigned the Pei sampling discrete FRFT method and proposed a new fast algorithm, i.e., sparse FRFT (SFRFT). Compared with the FRFT method, SFRFT improves the analysis efficiency of sparse signals under large data conditions, and has better performance on chirp signals. However, it is difficult to deal with high-order motion target (highly maneuvering) and the performance is seriously affected by clutter environment. Chen, et al., constructed the basic theoretical framework of sparse time-frequency distribution (STFD) [16] from the perspective of sparse optimization and decomposition, and proposed a short-time SFT (ST-SFT) and short-time SFRFT (ST-SFRFT)-based radar moving target detection method [29]–[32]. However, these methods are based on the optimization calculation, and it is difficult to guarantee the time requirement in case of large amount of data. Moreover, they need priori information of the sparse decomposition dictionary, which limits their applications in the detection of complex moving targets.

In this paper, in order to find a balance among the detection performance in clutter background, parameters estimation precision, and the computational cost, we proposed a detection method for maneuvering target via two-stage hierarchical detection in frequency and sparse domain. The first stage is the coarse detection processing screening out the range units having possible moving targets. The second stage is called the refined processing, and the robust SFRFT (RSFRFT) or robust sparse FRAF (RSFRAF) are proposed and used for moving target with different high-order motions, i.e., accelerated or jerk motion. The hierarchical processing method can achieve a good detection performance and at the same time reduce the computational burden greatly. The radar signal model of maneuvering target is established in Section II. In Section III, we introduce the principle of the two-stage processing. The flowchart of the proposed method and detailed analysis is shown in section IV. Finally, simulation results using real radar data and performances analysis are provided

in Section V. Section VI concludes the paper and gives future research direction.

II. ECHO MODEL OF MANEUVERING TARGET

For a coherent radar, the received radar returns are filtered and amplified and performed sampling for distance and azimuth directions respectively. Usually, the range sampling interval is equal to the radar range resolution, and the azimuth sampling frequency is equal to the pulse repetition frequency to ensure that the echo of the moving target can be completely acquired. Assuming that the radar and the target are in the same horizontal plane, the radar transmits a linear frequency modulation (LFM) signal.

$$s_t(t) = \text{rect}\left(\frac{t}{T_p}\right)\exp\left\{\text{j}2\pi\left[f_c t + \frac{1}{2}kt^2\right]\right\} \tag{1}$$

where $\text{rect}(u) = \begin{cases}1, & |u| \le 1/2\\ 0, & |u| > 1/2\end{cases}$, f_c is the radar carrier frequency, and T_p is the pulse width,

$$K_\alpha(t_m, u) = \begin{cases}A_\alpha \exp\left\{\text{j}\left[\frac{1}{2}t_m^2\cot\alpha - ut_m\csc\alpha + \frac{1}{2}u^2\cot\alpha\right]\right\}, & \alpha \ne n\pi\\ \delta\left[u-(-1)^n t_m\right], & \alpha = n\pi\end{cases}$$

means the frequency modulation (chirp rate), and B_n is the bandwidth. Then the received signal at time t is expressed as

$$s_r(t, t_m) = \sigma_r \text{rect}\left(\frac{t-\tau}{T_p}\right)\exp\left\{\text{j}2\pi\left[f_c(t-\tau)+\frac{k}{2}(t-\tau)^2\right]\right\} \tag{2}$$

where σ_r is the radar cross section (RCS), $\tau = 2R_s(t_m)/c_0$ is the time delay, c_0 represents the speed of light, t is the fast time within the pulse, and t_m is the slow time among pulses, $R_s(t_m)$ is the line-of-sight distance between the radar and the target.

Then the radar returns along the distance direction are demodulated, and the radar transmitting signal can be used as the demodulation reference signal.

$$s_{\text{IF}}(t, t_m) = s_r(t, t_m)\cdot s_t^*(t) \tag{3}$$

where '$*$' indicates the complex conjugate operation. The demodulated radar echo data are subjected to pulse compression processing to obtain radar echo data accumulated within the pulse.

$$s_{\text{PC}}(t, t_m) = A_r \text{sinc}\left[B\left(t - \frac{2R_s(t_m)}{c_0}\right)\right]\exp\left(-\text{j}\frac{4\pi R_s(t_m)}{\lambda}\right) \tag{4}$$

where $R_s(t_m)$ is the line-of-sight distance between the radar and the target, A_r is the amplitude of the echo, $2R_s(t_m)/c_0$ is the time delay, and λ is the wavelength of the signal.

Assuming that the target is moving towards the radar and the moving distance of target does not move across one rangebin or the range migration has been compensated. Only considering the radial velocity component, the distance of the target is a polynomial function of time.

$$R_{s_1}(t_m) = r_0 + v_0 t_m + a_s t_m^2/2 \tag{5}$$

$$R_{s_2}(t_m) = r_0 + v_0 t_m + a_s t_m^2/2 + g_s t_m^3/6 \tag{6}$$

where $R_{s_1}(t_m)$ and $R_{s_2}(t_m)$ represent the radial distance of the accelerated motion and high-order motion (jerk motion), respectively, r_0, v_0, a_s, and g_s are the initial distance, initial velocity, acceleration, and jerk parameters. Record the range-pulses two-dimensional data matrix, i.e.,

$$\mathbf{S}_{M\times N} = \{s_{\text{PC}}(i,j)|i=1,2,\ldots,M;\quad j=1,2,\ldots,N\} \tag{7}$$

where M and N are the number of rangebins and pulses.

III. PRINCIPLE OF THE HIERARCHICAL DETECTION FOR MANEUVERING TARGET

This section will introduce a fast and refined processing method of radar maneuvering target based on hierarchical detection, comprehensively utilizing the advantages of MTD, and sparse fractional representation, i.e., RSFRFT and RSFRAF. It adopts two-level threshold processing, that is, first we employ MTD processing under a higher false alarm probability (P_{fa}) condition threshold (first-level threshold), screening out the rangbins of possible moving targets, and then pass the echoes of these rangbins in parallel through RSFRFT and RSFRAF operations, and choose the more sparse one to represent the maneuvering target echoes. The constant false alarm detection (second level threshold) is performed in the corresponding range-optimal sparse fractional representation domain (SFRRD). Only a few rangbins exceeding the first level threshold are performed in the second detection stage. It would reduce the amount of calculation while ensuring high detection and estimation performance.

A. THE FIRST STAGE INTEGRATION DETECTION (COARSE PROCESSING)

Select $N_1 \in [2, N]$ pulses of the same rangebin from the range-pulses two-dimensional data matrix, and perform Fourier transform to realize pulse integration.

$$S_{\text{MTD}} = \int s_{\text{PC}}(t, t_m)\exp(-\text{j}2\pi f_{\text{d}} t_m)\text{d}t_m. \tag{8}$$

Then, compare the range-Doppler two-dimensional data $\mathbf{S}_{\text{MTD}} = \{S_{\text{MTD}}(i,j)|i=1,\ldots,M; j=1,\ldots,N_1\}$ with the detection threshold (low threshold) under higher P_{fa} (usually the P_{fa} is higher than 10^{-2}),

$$|\mathbf{S}_{\text{MTD}}| \underset{H_0}{\overset{H_1}{\gtrless}} \eta_1 \tag{9}$$

where η_1 is the threshold, determined by the P_{fa}.

Store the rangebin number whose outputs are higher than the first threshold (η_1), and the rangebins-pulses echo data corresponding to the first-level detection threshold is constructed from the output of $\mathbf{S}'_{M_1\times N}$.

$$\mathbf{S}'_{M_1\times N} = \left\{s'_{\text{PC}}(i,j)|i=1,2,\ldots,M_1; j=1,2,\ldots,N\right\} \tag{10}$$

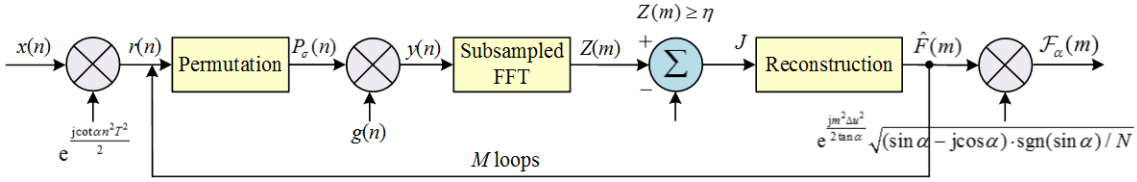

FIGURE 1. Flowchart of RSFRFT [33].

where M_1 indicates the number of rangbins that exceed the first level threshold.

B. THE SECOND STAGE DETECTION VIA SPARSE FRACTIONAL REPRESENTATION (REFINED PROCESSING)

1) ROBUST SFRFT (RSFRFT)

The SFRFT algorithm has good aggregation performance for LFM signals, and when the data length N is larger than 2^{10}, the computational complexity of FRFT can be significantly increased. However, SFRFT directly takes the frequency point corresponding to the top K extreme large values in the subsampling spectrum as the estimation result, wherein the sparsity K needs to be preset or roughly estimated, which is easy to be influenced by the clutter background. Therefore, in the background of the low SCR, the performance of the SFRFT algorithm will deteriorate, which will easily lead to false alarms. We combine the novelty of ADT-SFT in [27], and proposed the robust SFRFT (RSFRFT) [33], shown in Fig. 1, which is composed of seven procedures.

a: CHIRP1 MULTIPLICATION

Multiplying the echo signal $x(n)$ by the Chirp1 signal,

$$r(n) = x(n) \cdot \mathrm{e}^{\frac{j\cot\alpha n^2 T^2}{2}}, \quad n \in [1, N] \tag{11}$$

where $\mathrm{e}^{\frac{j\cot\alpha n^2 T^2}{2}}$ is a chirp signal, α is the rotation angle.

b: SPECTRUM PERMUTATION

In order to make the large-value frequency points as uniform and random as possible, the time domain signal is operated to realize spectrum permutation. The permutation mode is defined as P_σ, and the time serials after permutation can be defined as [20]

$$P_\sigma(n) = r[(\sigma n) \bmod N], \quad n \in [1, N] \tag{12}$$

where σ is a random odd number, and mod denotes the modulo operation.

c: FILTERING

Define a window function $g(n)$, and its spectrum $G(m)$ satisfies

$$G(m) \in \begin{cases} [1-\delta, 1+\delta], & m \in [-\varepsilon' N, \varepsilon' N] \\ [0, \delta], & m \notin [-\varepsilon N, \varepsilon N] \end{cases} \tag{13}$$

where ε' and ε denote the stopband factor and passband factor, respectively, and δ denotes the oscillation extent. The time domain signal after filtering can be expressed as

$$y(n) = g(n) \cdot P_\sigma(n), \quad n \in [1, N], \tag{14}$$

$\mathrm{supp}(y) \subseteq \mathrm{sup}\, p(g) = [-\omega/2, \omega/2]$, where supp represents the support and ω is the window length.

d: SUBSAMPLED-FFT

According to the property of FT, the subsampling in the frequency domain can be realized by aliasing in the time domain. Then the signal after subsampled-FFT is

$$\begin{aligned} Z(m) &= \mathrm{FFT}\{z(n)\} \\ &= \mathrm{FFT}\left\{ \sum_{j=0}^{\lfloor \omega/B \rfloor - 1} y(n + jB), n \in (1, B) \right\} \end{aligned} \tag{15}$$

where B is an integer, and N is divided by B, $\lfloor\rfloor$ is the rounding down operation.

e: ADAPTIVE SPARSITY DETERMINATION

The threshold is added after the subsampled FFT to estimate the signal sparsity and frequency points. In this way, there is no need to preset the sparsity K, and the coordinates corresponding to the frequency points in the $Z(m)$ whose amplitude exceeds the threshold are classified into the set J, that is,

$$J = \{m \in [1, B] \,|Z(m) \geq \eta\} \tag{16}$$

where η is the threshold, determined by the constant false alarm rate (CFAR) detection technology [34], [35].

f: RECONSTRUCTION

Define a hash function

$$h_\sigma(m) = \lfloor \sigma \cdot m \cdot B/N \rfloor \tag{17}$$

The corresponding coordinates of J in the spectrum sequence of the signal $r(n)$ are obtained by hash inverse mapping and are saved in the set U.

$$U = \{m \in [1, N] \,|h_\sigma(m) \in J\} \tag{18}$$

For more accurate results, M loops are needed in the reconstruction process. We define the occurrence threshold γ, and the frequency whose "occurrence number" exceeds γ in the loops, is identified as the suspicious target frequency.

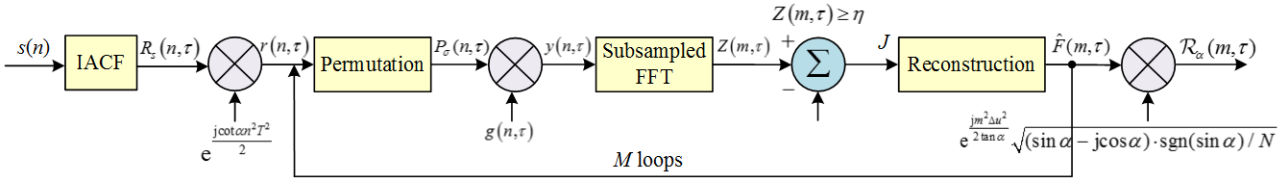

FIGURE 2. Flowchart of RSFRAF.

g: CHIRP2 MULTIPLICATION

Supposing the spectrum after reconstruction is $\hat{F}(m)$, the final result of RSFRFT is

$$\mathcal{F}_\alpha(m)=\hat{F}(m)\cdot \mathrm{e}^{\frac{\mathrm{j}m^2\Delta u^2}{2\tan\alpha}}\sqrt{(\sin\alpha-\mathrm{j}\cos\alpha)\cdot\mathrm{sgn}(\sin\alpha)/N} \tag{19}$$

where $\mathrm{e}^{\frac{\mathrm{j}m^2\Delta u^2}{2\tan\alpha}}\sqrt{(\sin\alpha-\mathrm{j}\cos\alpha)\cdot\mathrm{sgn}(\sin\alpha)/N}$ is chirp2 signal, sgn is the sign function, $\Delta u = 2\pi\Delta T\,|\sin\alpha|/N$ is the fractional domain sampling interval.

Procedure (2) to (6) is named as adaptive SFT (ASFT).

2) ROBUST SFRAF (RSFRAF)

The main process of RSFRAF is quite similar to RSFRFT, and the difference is that RSFRAF has a procedure which is called as the instantaneous autocorrelation function (IACF). The detailed procedure of RSFRAF is shown in Fig. 2. For a maneuvering target in clutter background modelled as quadratic frequency modulated (QFM) signal, the discrete signal can be expressed as

$$s(n\Delta t)=A_0\exp\left[\mathrm{j}2\pi\left(a_0+a_1n\Delta t+a_2n^2\Delta t^2+a_3n^3\Delta t^3\right)\right]+c(n\Delta t),\quad n\in[1,N] \tag{20}$$

where A_0 is the signal amplitude, $a_i(i=0,1,2,3)$ is the polynomial coefficients, i.e., $a_0=2R_0/\lambda$, $a_1=2v_0/\lambda$, $a_2=a_s/\lambda$, $a_3=g_s/3\lambda$, $\Delta t=1/f_s$ is the sampling interval, $N=T_n\cdot f_s$ is the sampling number, the observation time T_n, and the sampling frequency f_s, $c(n\Delta t)$ is the clutter.

The RSFRAF $\mathcal{R}_\alpha()$ with transform angle α is defined as follows,

$$\mathcal{R}_\alpha(m,\tau)=\mathcal{C}_m\left(\mathcal{S}\left[\mathcal{C}_n\left(\underbrace{R_s(n,\tau)}_{\text{IACF}}\right)\right]\right) \tag{21}$$

where $m\in[1,N]$ is the discrete variables in RSFRAF domain, $\mathcal{C}()$ and $\mathcal{S}()$ represent the chirp and ASFT operators respectively. $R_s()$ is the IACF calculation,

$$\begin{aligned}R_s(n,\tau)&=s(n\Delta t+\tau/2)s^*(n\Delta t-\tau/2)\\&=A_0^2\exp\left[\mathrm{j}2\pi\tau\left(a_1+2a_2n\Delta t+3a_3n^2\Delta t^2+a_3\tau^2/4\right)\right]+R_c(n,\tau)+R_{sc}(n,\tau)\end{aligned} \tag{22}$$

where τ is a time delay, $R_c(n,\tau)$ and $R_{sc}(n,\tau)$ are the IACF of auto-term of clutter and cross-terms between clutter and target.

After the IACF, the remaining procedure of RSFRAF is the same as the RSFRFT, and normally time delay is a constant value [2]. Supposing the spectrum after reconstruction is $\hat{F}(m)$, the final result of RSFRAF is $\mathcal{R}_\alpha(m)$.

IV. FAST AND REFINED PROCESSING OF RADAR MANEUVERING TARGET

The diagram of the proposed algorithm is shown in Fig. 3, which mainly includes six steps.

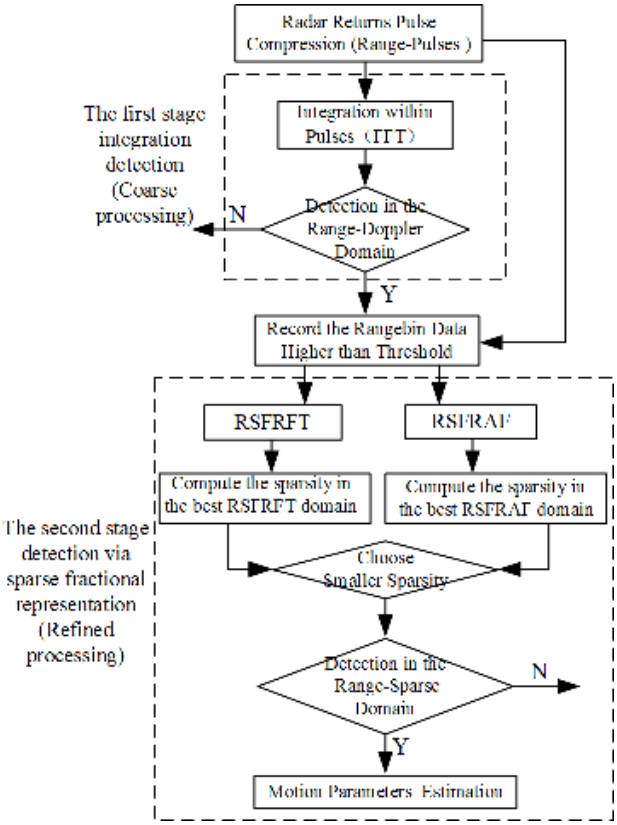

FIGURE 3. Flowchart of the RSFRFT-RSFRAF based hierarchical detection method.

Step 1: Perform the pulse compression for radar returns, and record the two-dimensional range-pulses data $\mathbf{S}_{M\times N}$.

Step 2: Perform the first stage integration detection (coarse processing), which has been described in section ćó(A). Then we obtain the data $\mathbf{S}'_{M_1\times N}$ whose values exceed the first level threshold.

Step 3: Perform the second stage detection via sparse fractional representation (refined processing). The $N_2 \in [2, N]$ sampled pulses of the same rangebin in the output of the first stage are performed RSFRFT and RSFRAF operations respectively, i.e., $\mathcal{F}_\alpha(m)$ and $\mathcal{R}_\alpha(m)$.

Step 4: In order to evaluate which sparse fractional representation has better performance for the maneuvering target, we define the output sparsity D (number of the output frequency points exceeding the adaptive threshold in (16))as the selection criteria. Since the RSFRFT is more effective for the uniformly moving target whose instantaneous range is (5) and RSFRAF is good at dealing with highly maneuvering target moving along the range (6), the sparsity of the two methods, i.e., D_{RSFRFT}, and D_{RSFRAF} will be different. Less sparsity (output frequency points) means the SFRRD could represent the maneuvering target more sparsely and precisely, which is of great benefit to signal integration. Calculate the sparsity of the best SFRRD at the distance r_i, i.e., $D_{\text{RSFRFT}}|_{r_i}$ and $D_{\text{RSFRAF}}|_{r_i}$. Then select the optimal sparse representation corresponding to a smaller D.

Step 5: All the rangebins are traverses and the $M_1 \times N_2$ dimensional range-optimal sparse domain matrix are constructed.

$$\mathbf{F}_{\alpha_{i_0}}(m) = \begin{bmatrix} \mathcal{F}_{\alpha_{1_0}}(1)|_{r_1}, \mathcal{F}_{\alpha_{1_0}}(2)|_{r_1}, \ldots, \mathcal{F}_{\alpha_{1_0}}(N_2)|_{r_1} \\ \mathcal{F}_{\alpha_{2_0}}(1)|_{r_2}, \mathcal{F}_{\alpha_{2_0}}(2)|_{r_2}, \ldots, \mathcal{F}_{\alpha_{2_0}}(N_2)|_{r_2} \\ \vdots \\ \mathcal{F}_{\alpha_{M_{1_0}}}(1)|_{r_{M_1}}, \mathcal{F}_{\alpha_{M_{1_0}}}(2)|_{r_{M_1}}, \ldots, \mathcal{F}_{\alpha_{M_{1_0}}}(N_2)|_{r_{M_1}} \end{bmatrix}_{M_1 \times N_2} \tag{23}$$

or

$$\mathbf{R}_{\alpha_{i_0}}(m) = \begin{bmatrix} \mathcal{R}_{\alpha_{1_0}}(1)|_{r_1}, \mathcal{R}_{\alpha_{1_0}}(2)|_{r_1}, \ldots, \mathcal{R}_{\alpha_{1_0}}(N_2)|_{r_1} \\ \mathcal{R}_{\alpha_{2_0}}(1)|_{r_2}, \mathcal{R}_{\alpha_{2_0}}(2)|_{r_2}, \ldots, \mathcal{R}_{\alpha_{2_0}}(N_2)|_{r_2} \\ \vdots \\ \mathcal{R}_{\alpha_{M_{1_0}}}(1)|_{r_{M_1}}, \mathcal{R}_{\alpha_{M_{1_0}}}(2)|_{r_{M_1}}, \ldots, \mathcal{R}_{\alpha_{M_{1_0}}}(N_2)|_{r_{M_1}} \end{bmatrix}_{M_1 \times N_2} \tag{24}$$

where $\mathcal{F}_\alpha(m)|_{r_i}$ and $\mathcal{R}_\alpha(m)|_{r_i}$ represents the RSFRFT and RSFRAF at the distance r_i, and then the optimal sparse domain is $\mathcal{F}_{\alpha_{i_0}}(m)|_{r_i}$ and $\mathcal{R}_{\alpha_{i_0}}(m)|_{r_i}$, respectively.

Step 6: Take $\mathbf{F}_{\alpha_{i_0}}(m)$ or $\mathbf{R}_{\alpha_{i_0}}(m)$ as the detection statistics and compare them with the threshold under the condition of low false alarm probability (P_{fa}, usually the false alarm probability is not higher than 10^{-3}) to complete the maneuvering target detection.

$$\left|\mathbf{F}_{\alpha_{i_0}}(m)\right| \underset{H_0}{\overset{H_1}{\gtrless}} \eta_2 \quad \text{or} \quad \left|\mathbf{R}_{\alpha_{i_0}}(m)\right| \underset{H_0}{\overset{H_1}{\gtrless}} \eta_3 \tag{25}$$

where η_2 and η_3 are the second detection threshold, which is determined by the P_{fa}. If the detection statistic is lower than the detection threshold, it indicates that the rangebin has no maneuvering target. If the detection statistic is higher than the detection threshold, it indicates that the rangebin has the maneuvering target.

V. SIMULATION AND RESULTS ANALYSIS

In this section, real radar data are used to verify the performance of the proposed algorithm in clutter background. Moreover, the detection performance is compared with hierarchical coherent integration using FRFT and FRAF (FRFT-FRAF-HCI). The computational burden is analyzed and simulated as well.

A. RADAR DATA DESCRIPTION

The experiment uses an X-band solid-state full-coherence navigation radar to observe a maneuvering unmanned aerial vehicle (UAV) target. The radar operates in a dwell mode and is able to obtain more pulses to increase the Doppler resolution of the target. The UAV target is a quadrotor drone, radial flying about 3-5 km from the radar. Fig. 4 shows the scenario and processing flow of the detection experiment. The radar is equipped at the top of a building near the sea, and the drone is flying in the sky. The background is complex due to the land, buildings and sea. The radar data is sampled and collected and then feed to the computer for further real time signal processing, and multisensors information including radar returns, optical, and infrared images are combined together to tracking the drone target.

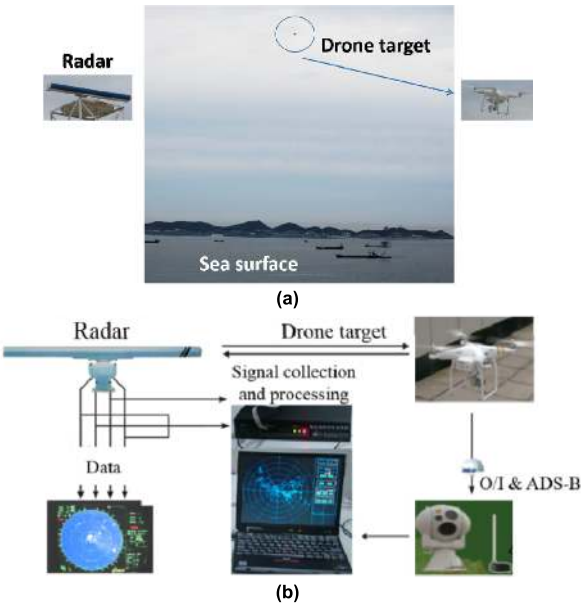

FIGURE 4. ***The experiment scene for*** **maneuvering** ***target observation.*** **(a) The experiment scene for drone maneuvering target observation,** ***(b)*** **Data processing for drone target observation with multisensors.**

Fig. 5 demonstrates the radar returns characteristics of the drone target. Form the Fig. 5(a) the range versus pulses image of initial radar returns in dB, it can be found that the clutter is stronger than the drone target. Then each rangibn is performed by 2048 points FFT and then we obtain Fig. 5(b),

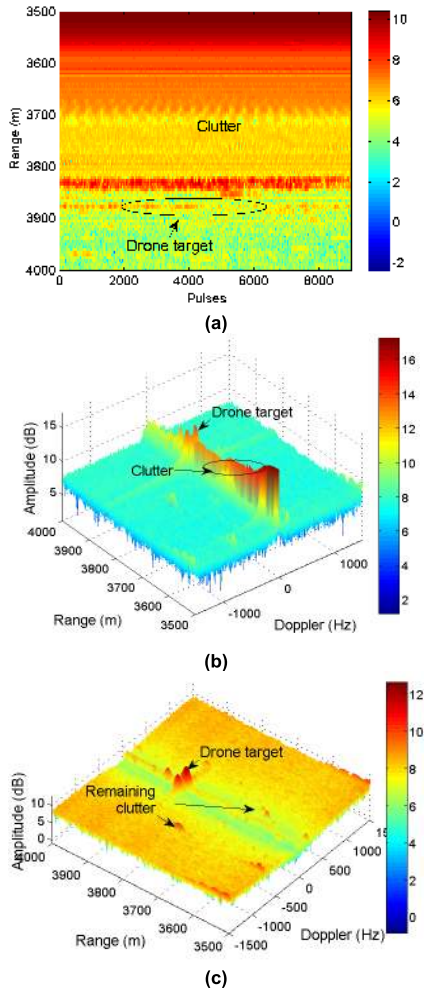

FIGURE 5. *Descriptions of radar returns of UAV target.* **(a) Range versus pulses image of initial radar returns (dB), (b) Range versus Doppler image (dB), $N = 2048$, (c) Range versus pulses image of radar returns after MTI (dB), $N = 2048$.**

which is the range versus Doppler image. The clutter spectrum is still very strong to overlap the target's Doppler amplitudes. Then, the moving target indication (MTI) is performed, and the result is shown in Fig. 5(c). The returns of the target are clear and the range is around 3850m to 3900m. However, there is still some residual clutter, which would influence the target detection.

Fig. 6 shows the detection result of the first stage with sampling number 2048. It can be seen from Fig. 6(a), i.e., range versus Doppler image (dB) after CFAR detection ($P_{\text{fa}} = 10^{-4}$) that there are only a few coefficients above the amplitude. The first stage is done by MTD, which is fast, while the resolution and energy integration ability are poor. Moreover, there is still some residue clutter in the biggest Doppler spectrum of rangebin 766 (Fig. 6(b)). Therefore, it still needs second detection for refined processing.

B. DETECTION COMPARISONS WITH FRFT-FRAF-HCI

In this part, we will compare with the proposed method with the coherent integration method, i.e., hierarchical coherent integration using FRFT and FRAF (FRFT-FRAF-HCI),

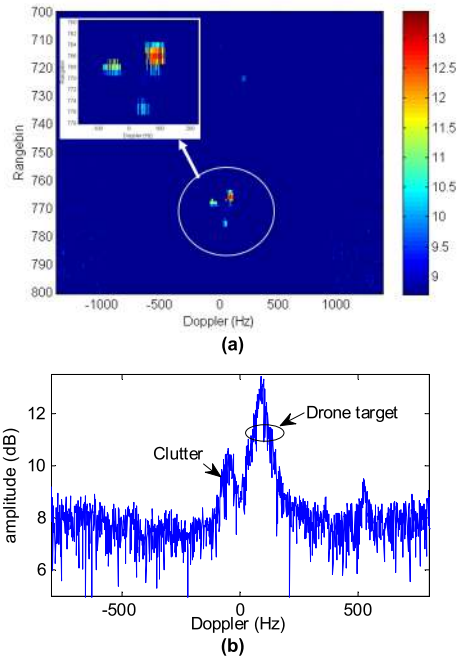

FIGURE 6. **Detection result of the first stage (N = 2048). (a) Range versus Doppler image (dB) after CFAR detection ($P_{\text{fa}} = 10^{-4}$), (b) Biggest Doppler spectrum of rangebin 766.**

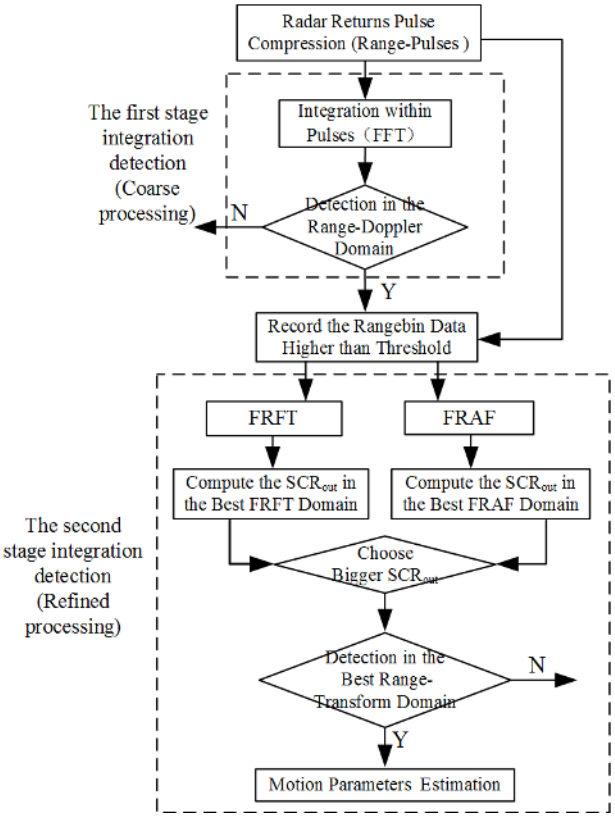

FIGURE 7. **Flowchart of the FRFT-FRAF-HCI based detection method.**

which is shown in Fig. 7. The $N_2 \in [2, N]$ sampled pulses of the same rangebin in the output of the first stage are performed FRFT and FRAF operations under different transform

angle conditions, i.e.,

$$S^{\alpha}_{\mathrm{FRFT}}(u) = \int S'_{\mathrm{PC}}(t, t_m) K_{\alpha}(t_m, u) \mathrm{d}t_m \tag{26}$$

$$S^{\alpha}_{\mathrm{FRAF}}(u) = \int S'_{\mathrm{PC}}(t, t_m + \tau_0/2) S'^{*}_{\mathrm{PC}}(t, t_m - \tau_0/2) \times K_{\alpha}(t_m, u) \mathrm{d}t_m \tag{27}$$

where $\alpha \in (-\pi, \pi]$ is the rotation angle, and τ_0 is a constant indicating the delay, which is determined by the initial distance r_0 of the target to be detected, i.e., $\tau_0 = 2r_0/c$, $K_{\alpha}(t_m, u)$ represents the kernel function.

$$K_{\alpha}(t_m, u) = \begin{cases} A_{\alpha} \exp\left\{ \mathrm{j} \left[\frac{1}{2} t_m^2 \cot\alpha - u t_m \csc\alpha + \frac{1}{2} u^2 \cot\alpha \right] \right\}, & \alpha \neq n\pi \\ \delta\left[u - (-1)^n t_m\right], & \alpha = n\pi \end{cases} \tag{28}$$

where $A_{\alpha} = \sqrt{(1 - \mathrm{j}\cot\alpha)/2\pi}$, and n is an integer.

For the target with uniform acceleration of a certain rangebin $r_i, i = 1, 2, \ldots, M_1$, its radar returns can be approximated as an LFM signal

$$f_1(t_m)|_{r_i} = A_{r_i} \exp\left[-\mathrm{j} \frac{4\pi}{\lambda} \left(r_i + v_{i_0} t_m + a_{i_0} t_m^2/2 \right) \right] = A_{r_i} \exp\left[-\mathrm{j} \left(\frac{4\pi}{\lambda} r_i + 2\pi f_{i_0} t_m + \pi \mu_{i_0} t_m^2 \right) \right] \tag{29}$$

where v_{i_0} is the initial velocity with the Doppler frequency $f_{i_0} = 2v_{i_0}/\lambda$, and a_{i_0} represents the acceleration with the chirp rate $\mu_{i_0} = 2a_{i_0}/\lambda$. It will form a peak in the FRFT domain, and the peak coordinates are as follows.

$$(\alpha_{i_0}, u_{i_0})|_{r_i} = \arg\max_{\alpha, u} \left| S^{\alpha}_{\mathrm{FRFT}}(u)|_{r_i} \right| = \left(-\mathrm{arc}\cot\mu_{i_0},\ f_{i_0} \sec\alpha_{i_0} \right)\big|_{r_i} \tag{30}$$

where $S^{\alpha}_{\mathrm{FRFT}}(u)|_{r_i}$ represents the FRFT at the distance r_i, and then the best FRFT domain is $S^{\alpha_{i_0}}_{\mathrm{FRFT}}(u)|_{r_i}$.

For the maneuvering target with high-order motion, its radar returns can be approximated as a QFM signal,

$$f_2(t_m)|_{r_i} = A_{r_i} \exp\left[-\mathrm{j} \frac{4\pi}{\lambda} \left(r_i + v_{i_0} t_m + a_{i_0} t_m^2/2 + g_{i_0} t_m^3/6 \right) \right] = A_{r_i} \exp\left[-\mathrm{j} \left(\frac{4\pi}{\lambda} r_i + 2\pi f_{i_0} t_m + \pi \mu_{i_0} t_m^2 + \pi k_{i_0} t_m^3/3 \right) \right] \tag{31}$$

where $k_{i_0} = 2g_{i_0}/\lambda$ is the change of the chirp rate corresponding to the jerk motion g_{i_0}. It will form a peak in the FRAF domain, and the peak coordinates are as follows.

$$(\alpha_{i_0}, u_{i_0})|_{r_i} = \arg\max_{\alpha, u} \left| S^{\alpha}_{\mathrm{FRAF}}(u)|_{r_i} \right| = \left(-\mathrm{arccot}(k_{i_0}\tau_i),\ \mu_{i_0}\tau_i \sin\alpha_{i_0} \right), \quad \alpha_{i_0} \neq (2n-1)\pi/2 \tag{32}$$

where $S^{\alpha}_{\mathrm{FRAF}}(u)|_{r_i}$ represents the FRAF at the distance r_i, and then the best FRFT domain is $S^{\alpha_{i_0}}_{\mathrm{FRAF}}(u)|_{r_i}$.

It can be known from (30) and (32) that if the moving target to be detected is an accelerated moving target, the energy can be optimally aggregated as a peak in the best FRFT domain, while the highly maneuvering target with jerk motion cannot obtain good accumulation. On the other hand, only if the moving target to be detected is a maneuvering target with jerk motion, the energy can be optimally aggregated as a peak in the best FRAF domain. Although a peak can be formed in the FRAF domain for the accelerated moving target, the peak is located at $\alpha_{i_0} = (2n-1)\pi/2$, and it is easy to alias with the peaks of clutter or noise, which is not conducive to detection.

Perform the second stage integration detection (refined processing). The optimal result selection criteria between the FRFT-FRAF-HCI detection and the RSFRFT-RSFRAF based detection method is different. Define the output SCR in the optimal transform domain ($\mathrm{SCR}_{\mathrm{out}}$) as

$$\mathrm{SCR}_{\mathrm{TD}} = 10\lg \frac{\frac{1}{2d} \sum_{l-d}^{l+d} |y(i)|^2}{\frac{1}{N_2 - 2d} \left[\sum_{1}^{l-d} |y(i)|^2 + \sum_{l+d}^{N_2} |y(i)|^2 \right]} \tag{33}$$

Equ. (33) represents the ratio of target energy to clutter or noise energy, $y(i)$ is the optimum FRFT domain or the best FRAF domain, and l is the maximum peak location, $d = \pi f_s \sin\alpha_{i_0}/N_2$ is half of the peak width, f_s is the sampling frequency.

Then calculate the $\mathrm{SCR}_{\mathrm{TD}}$ of the best FRFT and FRAF domain respectively, i.e., $\mathrm{SCR}_{\mathrm{FRFT}}|_{r_i}$ and $\mathrm{SCR}_{\mathrm{FRAF}}|_{r_i}$, and select the optimal transform domain corresponding to the larger $\mathrm{SCR}_{\mathrm{TD}}$. All the rangebins are traversed and $M_1 \times N_2$ dimensional range versus optimal transform domain matrix is constructed.

$$\mathbf{S}^{\alpha_{i_0}}_{\mathrm{FRFT}}(u) = \begin{bmatrix} S^{\alpha_{1_0}}_{\mathrm{FRFT}}(1)|_{r_1}, S^{\alpha_{1_0}}_{\mathrm{FRFT}}(2)|_{r_1}, \ldots, S^{\alpha_{1_0}}_{\mathrm{FRFT}}(N_2)|_{r_1} \\ S^{\alpha_{2_0}}_{\mathrm{FRFT}}(1)|_{r_2}, S^{\alpha_{2_0}}_{\mathrm{FRFT}}(2)|_{r_2}, \ldots, S^{\alpha_{2_0}}_{\mathrm{FRFT}}(N_2)|_{r_2} \\ \vdots \\ S^{\alpha_{M_{1_0}}}_{\mathrm{FRFT}}(1)|_{r_{M_1}}, S^{\alpha_{M_{1_0}}}_{\mathrm{FRFT}}(2)|_{r_{M_1}}, \ldots, S^{\alpha_{M_{1_0}}}_{\mathrm{FRFT}}(N_2)|_{r_{M_1}} \end{bmatrix}_{M_1 \times N_2} \tag{34}$$

or

$$\mathbf{S}^{\alpha_{i_0}}_{\mathrm{FRAF}}(u) = \begin{bmatrix} S^{\alpha_{1_0}}_{\mathrm{FRAF}}(1)|_{r_1}, S^{\alpha_{1_0}}_{\mathrm{FRAF}}(2)|_{r_1}, \ldots, S^{\alpha_{1_0}}_{\mathrm{FRAF}}(N_2)|_{r_1} \\ S^{\alpha_{2_0}}_{\mathrm{FRAF}}(1)|_{r_2}, S^{\alpha_{2_0}}_{\mathrm{FRAF}}(2)|_{r_2}, \ldots, S^{\alpha_{2_0}}_{\mathrm{FRAF}}(N_2)|_{r_2} \\ \vdots \\ S^{\alpha_{M_{1_0}}}_{\mathrm{FRAF}}(1)|_{r_{M_1}}, S^{\alpha_{M_{1_0}}}_{\mathrm{FRAF}}(2)|_{r_{M_1}}, \ldots, S^{\alpha_{M_{1_0}}}_{\mathrm{FRAF}}(N_2)|_{r_{M_1}} \end{bmatrix}_{M_1 \times N_2} \tag{35}$$

TABLE 1. Detection performances of different methods (high-order motion, Gaussian noise, $P_{fa} = 10^{-4}$).

Detection methods	MTD	FRFT-FRAF HCI	ASFT	RFRFT	RFRAF	RSFRFT-RSFRAF
N=2048, P_d (SNR=-5 dB)	57.2%	83.4% (Time=3.04s)	60.6%	72.8%	81.7%	86.9% (Time=1.79s)
N=2048, P_d (SNR=-10 dB)	30.1%	72.7% (Time=3.11s)	31.7%	65.4%	70.2%	71.3% (Time=1.81s)
N=8192, P_d (SNR=-5 dB)	64.7%	92.6% (Time=6.57s)	63.4%	79.6%	88.7%	93.8% (Time=2.56s)
N=8192, P_d (SNR=-10 dB)	44.8%	77.9% (Time=6.49s)	46.7%	70.4%	73.6%	77.4% (Time=2.61s)

*Computer configuration: Intel Core i7-4790 3.6GHz CPU; 16G RAM; Matlab 2014a.

Take $\mathbf{S}_{\mathrm{FRFT}}^{\alpha_{i_0}}(u)$ or $\mathbf{S}_{\mathrm{FRAF}}^{\alpha_{i_0}}(u)$ as the detection statistics and compare them with the threshold under the same P_{fa}.

$$\left|\mathbf{S}_{\mathrm{FRFT}}^{\alpha_{i_0}}(u)\right| \underset{H_0}{\overset{H_1}{\gtrless}} \eta_3 \quad \text{or} \quad \left|\mathbf{S}_{\mathrm{FRAF}}^{\alpha_{i_0}}(u)\right| \underset{H_0}{\overset{H_1}{\gtrless}} \eta_3 \tag{36}$$

where η_3 is the detection threshold.

Estimate the motion parameters of the maneuvering target according to the peak coordinate of the optimal fractional transform. For the uniformly moving target, the best FRFT domain peak coordinate is (α_{i_0}, u_{i_0}), then the target initial velocity estimation $\hat{v}_{l_0}$ and acceleration estimation $\hat{a}_{l_0}$ are

$$\begin{cases} \hat{v}_{l_0} = (\lambda/2)u_{l_0}\csc\alpha_{l_0} \\ \hat{a}_{l_0} = -(\lambda/2)\cot\alpha_{l_0} \end{cases} \tag{37}$$

For the nonuniform acceleration, the best FRAF domain peak coordinate is (α_{i_0}, u_{i_0}), then the target's acceleration estimation $\hat{a}_{l_0}$ and jerk estimation $\hat{g}_{i_0}$ are

$$\begin{cases} \hat{a}_{l_0} = (\lambda/2\tau_i)u_{l_0}\csc\alpha_{l_0} \\ \hat{g}_{i_0} = -(\lambda/2\tau_i)\cot\alpha_{l_0} \end{cases} \tag{38}$$

The initial frequency $\hat{f}_0$ can be estimated by dechirp calculation and searching the peak value of its spectrum [2].

The motion parameters estimation method of RSFRFT-RSFRAF hierarchical detection is similar with FRFT-FRAF-HCI, the different is that the peak coordinate is the biggest sparse value in the SFRRD

Based on the results of the first coarse detection stage of the measured data, the performance of the FRFT-FRAF HCI and the proposed method are further compared, as shown in Fig. 8. Comparing the FRFT and FRAF spectrum of the rangbin 766 where the maximum amplitude is located, i.e., Fig. 8(a) and Fig. 8(b), it can be seen that FRFT and FRAF have certain energy concentration ability on the maneuvering target compared with MTD. The integration gain is improved, and the $\mathrm{SCR}_{\mathrm{out}}$ is calculated according to (33), i.e., $\mathrm{SCR}_{\mathrm{FRFT}} = 16.04$ dB and $\mathrm{SCR}_{\mathrm{FRAF}} = 12.08$ dB. Therefore, the FRFT corresponding to the maximum output SCR is selected as the second stage of the refined processing. The final coherent integration result is shown in Fig. 8(c). Although the target peak is obvious, the FRFT spectrum is still broadened and the clutter energy is distributed in the FRFT domain as well. Using the proposed SFRRD processing method, the RSFRFT and RSFRAF spectrum are shown in Fig. 8(d) and Fig. 8(e). The sparsity of the two

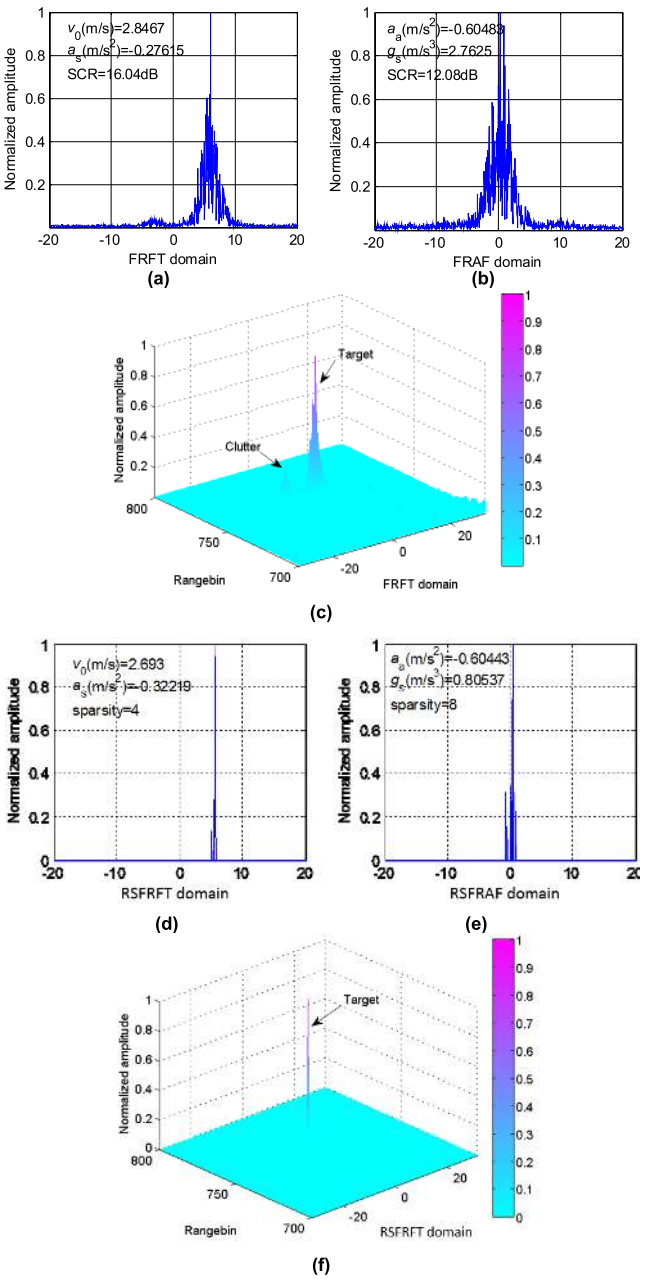

FIGURE 8. Flowchart of the FRFT-FRAF-HCI based detection method.

method is 4 and 8, respectively, and then select RSFRFT as the second stage of the refined detection method. The final processing result is shown in Fig. 8(f) according to

Fig. 3. By comparison, the proposed method only detects the target in its most sparse domain, thereby achieving clutter suppression.

C. DETECTION PERFORMANCES ANALYSIS

The detection performances of the proposed method and other integration methods, i.e., MTD, FRFT-FRAF HCI, ASFT, SFRFT, SFRAF, RSFRFT-RSFRAF, etc., are then compared in Table 1 ($P_{\text{fa}} = 10^{-4}$) by Monte Carlo trials. 10^6 times of experiments are carried out to obtain the detection probability. The moving target with high-order motion, i.e., QFM signal is simulated embedded in the Gaussian noise background. We can draw some conclusions from Table 1:

1) For the same sampling number and higher SCR (SCR $= -5$dB), the detection performance from high to low is: RSFRFT-RSFRAF, FRFT-FRAF HCI, SFRAF, SFRFT, ASFT, and MTD. While for lower SCR (SCR $= -10$dB), the detection performance from high to low is: FRFT-FRAF HCI, RSFRFT-RSFRAF, SFRAF, SFRFT, and ASFT≈MTD. This is because that the sparsity of SFRRD is affected by noise, resulting in worse performance under low SNR conditions.
2) For the different sampling number, longer observation or more pulses is helpful for higher detection performance.
3) Thanks to the SFT, the proposed method can significantly improve computational efficiency. Therefore, it requires much lower computational load than the FRFT-FRAF HCI, which is suitable for real applications.

From the above analysis, the advantages of the proposed method are that it can achieve high detection performance with less computational burden. However, it should be noted that the sparse representation and down sampling processing would be affected by noise or clutter, and in case of lower SCR, the performance of SFRFD-based method is close to or a little bit poorer than the coherent integration method.

D. COMPLEXITY ANALYSIS

Compared with the FRFT and FRAF algorithm, the RSFRFT and RSFRAF can quickly determine the Doppler frequencies of the suspected target due to the ASFT, which can reduce the computational burden in case of a large amount of data.

1) FRFT AND RSFRFT

The DFRFT-based method needs to search all the Doppler channels to establish the detector. Generally, if $\alpha \neq n\pi$ (n is an integer), the Pei's discrete FRFT can be seen as two times of multiplication with chirp signals and one time of FFT. Therefore, the overall multiplication complexity of FRFT is

$$O\left(2N + N/2\log_2 N\right) \tag{39}$$

The complex multiplication number of RSFRFT is

$$\text{RSFRFT}_{\#} \approx 2N + [w + B\log_2 B/2 + K + \text{card}(U)] \cdot M \tag{40}$$

where $B = O(\sqrt{N})$ is the length of sub-sampled FFT, $w = O(B\log_2 N)$ is the window length, K denotes the estimated sparsity obtained by the first level detection, set U contains the reconstructed frequency coordinates, card() denotes the cardinality of a set, P is the number of loops.

2) FRAF and RSFRAF

FRAF can be seen as the combination of IACF calculation and FRFT, and the multiplication of IACF is N. So the overall multiplication complexity of FRAF is

$$O\left(3N + N/2\log_2 N\right) \tag{41}$$

Similarly, the complex multiplication number of RSFRAF algorithm is about

$$\text{RSFRAF}_{\#} \approx 3N + [w + B\log_2 B/2 + K + \text{card}(U)] \cdot M \tag{42}$$

Complexity simulations of FRFT, FRAF, RSFRFT, and RSFRAF with different sparsity is shown in Fig. 9. It can be found that with the increase of pulse number, the efficiency property of RSFRFT and RSFRAF is more obvious. For example, when pulse number is 2^{14}, the complexity of FRFT is 147456, while RSFRFT with $K = 2$ is 57500, and $K = 20$ is 124900. when pulse number is 2^{16}, the complexity of FRFT is 655360, while RSFRFT with $K = 2$ is 172400, and $K = 20$ is 239800. And the increment of the complexity due to the sparsity is not obvious especially for large amount data. From the above analysis, the proposed method shows

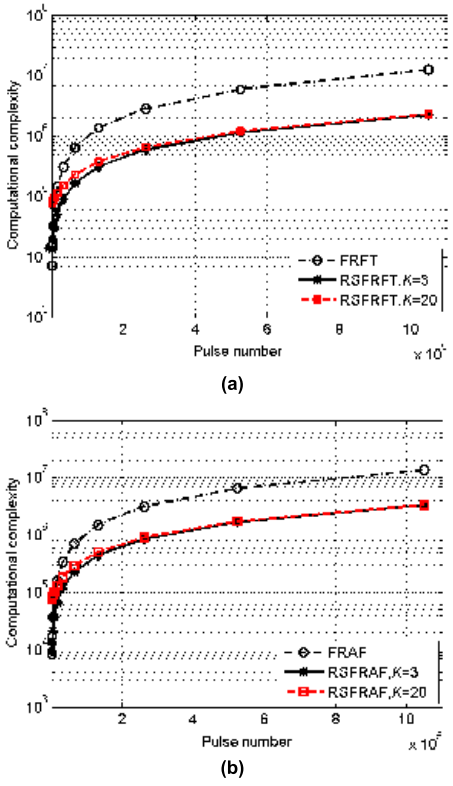

FIGURE 9. Complexity simulations of FRFT, FRAF, RSFRFT, and RSFRAF with different sparsity. (a) FRFT and RSFRFT. (b) FRAF and RSFRAF.

superior detection performance and can significantly reduce the computational complexity compared to the FRFT-FRAF HCI method.

VI. CONCLUSION

In this paper, we proposed a detection method for maneuvering target via two-stage hierarchical detection. The first stage is for the coarse detection and only these rangebins higher than the first threshold are carried out further processing. And the second stage is for the refined integration and detection using RSFRFT and RSFRAF according to the signal sparsity. Finally, radar experiment with UAV target are used for verification of the proposed method, which shows better performance than the traditional coherent integration method, e.g., MTD, FRFT, FRAF, and classical SFT based method. The proposed method only processes in a few rangebins which are determined by the first threshold, thereby reducing the amount of calculation while ensuring higher detection performance, and accurate motion parameters estimation of the maneuvering target, such as speed, acceleration and jerk, etc.. Then rapid and refined detection of maneuvering targets can be achieved. Long-time processing for more complex motion across rangbins will be analyzed in the future.

ACKNOWLEDGMENT

The authors would like to thank the anonymous reviewers for the valuable comments and suggestions.

REFERENCES

[1] J. Xu, J. Yu, Y.-N. Peng, and X.-G. Xia, "Radon-Fourier transform for radar target detection, I: Generalized Doppler filter bank," *IEEE Trans. Aerosp. Electron. Syst.*, vol. 47, no. 2, pp. 1186–1202, Apr. 2011.

[2] X. Chen, Y. Huang, N. Liu, J. Guan, and Y. He, "Radon-fractional ambiguity function-based detection method of low-observable maneuvering target," *IEEE Trans. Aerosp. Electron. Syst.*, vol. 51, no. 2, pp. 815–833, Apr. 2015.

[3] X. Chen, J. Guan, Z. Bao, and Y. He, "Detection and extraction of target with micromotion in spiky sea clutter via short-time fractional Fourier transform," *IEEE Trans. Geosci. Remote Sens.*, vol. 52, no. 2, pp. 1002–1018, Feb. 2014.

[4] X. Chen, B. Chen, Y. Huang, Y. He, and J. Guan, "Space-range-Doppler focus-based low-observable moving target detection using frequency diverse array MIMO radar," *IEEE Access*, vol. 6, pp. 43892–43904, 2018.

[5] X. Chen, J. Guan, N. Liu, and Y. He, "Maneuvering target detection via radon-fractional Fourier transform-based long-time coherent integration," *IEEE Trans. Signal Process.*, vol. 62, no. 4, pp. 939–953, Feb. 2014.

[6] J. Zheng, T. Su, L. Zhang, W. Zhu, and Q. H. Liu, "ISAR imaging of targets with complex motion based on the chirp rate–quadratic chirp rate distribution," *IEEE Trans. Geosci. Remote Sens.*, vol. 52, no. 11, pp. 7276–7289, Nov. 2014.

[7] P. Huang, G. Liao, Z. Yang, X.-G. Xia, J.-T. Ma, and J. Ma, "Long-time coherent integration for weak maneuvering target detection and high-order motion parameter estimation based on keystone transform," *IEEE Trans. Signal Process.*, vol. 64, no. 15, pp. 4013–4026, Aug. 2016.

[8] X. Rao, H. Tao, J. Xie, J. Su, and W. Li, "Long-time coherent integration detection of weak manoeuvring target via integration algorithm, improved axis rotation discrete chirp-Fourier transform," *IET Radar Sonar Navigat.*, vol. 9, no. 7, pp. 917–926, Aug. 2015.

[9] S.-N. Shi and P.-L. Shui, "Sea-surface floating small target detection by one-class classifier in time-frequency feature space," *IEEE Trans. Geosci. Remote Sens.*, vol. 56, no. 11, pp. 6395–6411, Nov. 2018.

[10] L. Zuo, M. Li, X. Zhang, Y. Wang, and Y. Wu, "An efficient method for detecting slow-moving weak targets in sea clutter based on time–frequency iteration decomposition," *IEEE Trans. Geosci. Remote Sens.*, vol. 51, no. 6, pp. 3659–3672, Jun. 2013.

[11] Q. He, N. H. Lehmann, R. S. Blum, and A. M. Haimovich, "MIMO radar moving target detection in homogeneous clutter," *IEEE Trans. Aerosp. Electron. Syst.*, vol. 46, no. 3, pp. 1290–1301, Jul. 2010.

[12] P. Wang, H. Li, and B. Himed, "Moving target detection using distributed MIMO radar in clutter with nonhomogeneous power," *IEEE Trans. Signal Process.*, vol. 59, no. 10, pp. 4809–4820, Oct. 2011.

[13] X. Li, G. Cui, W. Yi, and L. Kong, "Coherent integration for maneuvering target detection based on radon-Lv's distribution," *IEEE Signal Process. Lett.*, vol. 22, no. 9, pp. 1467–1471, Sep. 2015.

[14] R. Tao, Y.-L. Li, and Y. Wang, "Short-time fractional Fourier transform and its applications," *IEEE Trans. Signal Process.*, vol. 58, no. 5, pp. 2568–2580, May 2010.

[15] R. Tao, F. Zhang, and Y. Wang, "Fractional power spectrum," *IEEE Trans. Signal Process.*, vol. 56, no. 9, pp. 4199–4206, Sep. 2008.

[16] A. Gholami, "Sparse time–frequency decomposition and some applications," *IEEE Trans. Geosci. Remote Sens.*, vol. 51, no. 6, pp. 3598–3604, Jun. 2013.

[17] P. Flandrin and P. Borgnat, "Time-frequency energy distributions meet compressed sensing," *IEEE Trans. Signal Process.*, vol. 58, no. 6, pp. 2974–2982, Jun. 2010.

[18] X. Chen, J. Guan, Y. He, and X. Yu, "High-resolution sparse representation and its applications in radar moving target detection," *J. Radars*, vol. 6, no. 3, pp. 239–251, 2017.

[19] Z. Zhang, Y. Xu, J. Yang, X. Li, and D. Zhang, "A survey of sparse representation: Algorithms and applications," *IEEE Access*, vol. 3, no. 1, pp. 490–530, May 2015.

[20] H. Hassanieh, P. Indyk, D. Katabi, and E. Price, "Simple and practical algorithm for sparse Fourier transform," in *Proc. 23rd Annu. ACM-SIAM Symp. Discrete Algorithms*, Kyoto, Japan, Jan. 2012, pp. 1183–1194.

[21] H. Hassanieh, P. Indyk, D. Katabi, and E. Price, "Nearly optimal sparse Fourier transform," in *Proc. 44th Annu. ACM Symp. Theory Comput.*, New York, NY, USA, May 2012, pp. 563–578.

[22] J. Schumacher, "High performance sparse fast Fourier transform," M.S. thesis, Dept. Comput. Sci., ETH Zürich, Zürich, Switzerland, 2013.

[23] A. C. Gilbert, P. Indyk, M. Iwen, and L. Schmidt, "Recent developments in the sparse Fourier transform: A compressed Fourier transform for big data," *IEEE Signal Process. Mag.*, vol. 31, no. 5, pp. 91–100, Sep. 2014.

[24] C. Pang, S. Liu, and Y. Han, "High-speed target detection algorithm based on sparse Fourier transform," *IEEE Access*, vol. 6, pp. 37828–37836, 2018.

[25] G.-L. Chen, S.-H. Tsai, and K.-J. Yang, "On performance of sparse fast Fourier transform and enhancement algorithm," *IEEE Trans. Signal Process.*, vol. 65, no. 21, pp. 5716–5729, Nov. 2017.

[26] S. Wang, V. M. Patel, and A. Petropulu, "The robust sparse Fourier transform (RSFT) and its application in radar signal processing," *IEEE Trans. Aerosp. Electron. Syst.*, vol. 53, no. 6, pp. 2735–2755, Dec. 2017.

[27] X. Yu, X. Chen, Y. Huang, L. Zhang, J. Guan, and Y. He, "Radar moving target detection in clutter background via adaptive dual-threshold sparse Fourier transform," *IEEE Access*, vol. 7, pp. 58200–58211, 2019.

[28] S. Liu, T. Shan, R. Tao, Y. D. Zhang, G. Zhang, F. Zhang, and Y. Wang, "Sparse discrete fractional Fourier transform and its applications," *IEEE Trans. Signal Process.*, vol. 62, no. 24, pp. 6582–6595, Dec. 2014.

[29] X. Chen, J. Guan, X. Yu, and Y. He, "Radar detection for moving target in short-time sparse fractional Fourier transform domain," *Acta Electron. Sinica*, vol. 45, no. 12, pp. 3030–3036, 2017.

[30] X. Yu, X. Chen, Y. Huang, and J. Guan, "Sparse fractional Fourier transform and its applications in radar moving target detection," in *Proc. Int. Conf. Radar (RADAR)*, Brisbane, QLD, Australia, Aug. 2018, pp. 1–5.

[31] X. Chen, Y. Huang, J. Guan, and Y. He, "Radar micro-Doppler signal detection and extraction via short-time sparse fractional Fourier transform," in *Proc. Int. Conf. Radar Syst. (Radar)*, Belfast, U.K., Oct. 2017, pp. 1–4.

[32] X. Chen, X. Yu, J. Guan, and Y. He, "An effective and efficient long-time coherent integration method for highly maneuvering radar target in sparse domain," in *Proc. 4th Int. Workshop Compressed Sens. Theory Appl. Radar, Sonar Remote Sens. (CoSeRa)*, Aachen, Germany, Sep. 2016, pp. 124–127.

[33] X. Yu, X. Chen, Y. Huang, and J. Guan, "Fast detection method for low-observable maneuvering target via robust sparse fractional Fourier transform," *IEEE Geosci. Remote Sens. Lett.*, to be published. doi: 10.1109/LGRS.2019.2939264.

[34] H. Rohling, "Radar CFAR thresholding in clutter and multiple target situations," *IEEE Trans. Aerosp. Electron. Syst.*, vol. 19, no. 4, pp. 608–621, Jul. 1983.
[35] M. E. Smith and P. K. Varshney, "Intelligent CFAR processor based on data variability," *IEEE Trans. Aerosp. Electron. Syst.*, vol. 36, no. 3, pp. 837–847, Jul. 2000.

XIAOLONG CHEN (M'12) was born in Yantai, Shandong, China, in 1985. He received the bachelor's and master's degrees in signal and information processing, in 2010, and the Ph.D. degree in radar signal processing, in 2014, from Naval Aviation University (NAU), where he is currently an Associate Professor.

From 2015 to 2017, he was a Lecturer with the Marine Target Detection Research Group, NAU, where he lectures radar principle. He has given more than 20 speeches of radar signal processing, especially marine target. He has published more than 70 academic articles, two books, and holds 28 national invention patents. His current research interests include radar signal processing, especially for marine target detection, moving target detection, micro-Doppler, and clutter suppression.

In 2016, Dr. Chen was selected in the Young Talents Program of China Association for Science and Technology (CAST) and received the Excellent Doctor Dissertation of CIE. In 2017, he received the Chinese Patent Award. He received four excellent paper awards at 2016 International Radar Conference, 2017 EAI International Conference on Machine Learning and Intelligent Communications (MLICOM 2017), the 14th National Radar Conference, and 2019 IEEE 2nd International Conference on Electronic Information and Communication Technology (ICEICT 2019), respectively. In 2017 and 2018, his articles were selected as highly cited article of *Journal of Radars*, and F5000 Top Articles from *Outstanding S&T Journals of China*. In 2019, he received the Civil-military Integration Award of China Industry-University-Research Institute Collaboration Association (CIUR). He was selected for the Young Scientist Award at 2019 URSI Asia-Pacific Radio Science Conference and at 2019 International Applied Computational Electromagnetics Society Symposium, China (ACES). He was the TPC member of the 2015 and 2018 IET International Radar Conference. He has been the Committee Member of CIE Youth Commission and the Vice Executive Secretary of Radar and Information System Committee of CIE Young Scientist Club, since 2018. He was the Section Chair of 2016 International Conference on Mathematical Characterization, Analysis and Applications of Complex Information, 2017 MLICOM, 2017 International Conference on Radar Systems (UK), 2019 ICEICT, and 2019 ACES. He is the organizer of the special session Recent Development on Radar Signal Processing of 2019 ICEICT, special session Radar Marine Target Detection and Recognition of ACES 2019, and workshop Advances in Radar Signal Processing and Target Recognition of International Conferences on Communications Signal Processing and Systems (CSPS 2019). He has been in the Editorial Board of *Journal of Radars*, since 2019, and has been an Associate Editor of IEEE Access, since 2018. He is the Reviewer for the IEEE TSP, IEEE SPL, IEEE TGRS, IEEE GRSL, IEEE JSTARS, IET RSN, IET SP, IET EL, DSP, and many international conferences.

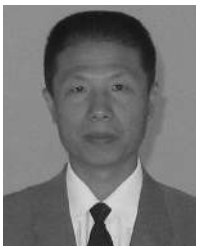

JIAN GUAN (M'07) received the Ph.D. degree in electronic engineering from Tsinghua University, Beijing, China, in 2000.

He is currently a Professor with NAU. He has authored numerous articles in his areas of expertise and holds 21 national invention patents. He is the author of two books related to radar detection. His research interests include radar target detection and tracking, image processing, and information fusion.

Dr. Guan is a Senior Member of the CIE and a Committee Member of Radio Positioning Technology Branch in CIE. He received the prize of the National Excellent Doctoral Dissertation, Realistic Outstanding Youth Practical Engineering Award of CAST and was selected for National Talents Engineering of Ministry of Personnel of China. He is in the Editorial Boards of many radar-related journals. He has served in the technical committee of many international conferences on radar.

GUOQING WANG was born in Anqiu, Shandong, China, in 1980. He received the Ph.D. degree from the National University of Defense Technology, Information and Communication Engineering, in 2010.

He is currently a Lecturer with NAU. His current research interests include high-speed signal acquisition and radar signal processing.

HAO DING was born in 1988. He received the bachelor's and master's degrees in signal and information processing, in 2012, and the Ph.D. degree, in 2016, from Naval Aviation University (NAU). He is the key member of marine target detection research group with the information fusion research group, NAU. He has published more than 30 academic articles, and he held about ten national invention patents and one software copyright. His research interest includes radar sea clutter property cognition, suppression, and target detection techniques.

In 2014, he received excellent master's dissertation of Shandong province. In 2018, he was selected as the Young Talents Program of CAST, and he received the first prize of postgraduate outstanding scientific and technological innovation achievement award of Shandong province. His main research achievements won the first prize of scientific and technological progress award, in 2018. He has attended the European Microwave Week International Conference, the IEEE Radar Conference, and so on, and given academic reports. He acts as a Reviewer for many international journals and conferences.

YONG HUANG was born in Hunan, China, in 1979. He received the M.S. and Ph.D. degrees in information and communication engineering from NAU, in 2005 and 2010, respectively, where he is currently an Associate Professor. From 2011 to 2016, he was a Lecturer with the Department of Electronic and Information Engineering, NAU.

His current research interests include radar signal processing and clutter rejection.